ADVANCED FUNCTIONAL MATERIALS
www.afm-journal.de

CART: Carrier-Based Actuatable and Reprogrammable Transport

Nikolaj K. Mandsberg, Julian A. Serna, and Pavel A. Levkin**

Remote manipulation of microcargo is essential for miniaturized automated experiments in fields such as biology, chemistry, and diagnostics, allowing efficient use of scarce, expensive, or hazardous materials. Current methods for manipulating microcargo are generally limited to droplets as cargo and rely on reduced substrate-cargo friction and special substrate-cargo interactions (electrowetting, anisotropic wetting, water-repellency, etc.) to enable cargo mobility. This limits the versatility of substrate and cargo choice. Here, CART (Carrier-based Actuatable and Reprogrammable Transport) is presented as a solution to these challenges. By introducing a carrier between the substrate and the cargo, CART physically separates them, eliminating the need to reduce substrate-cargo friction and the need for substrate-cargo matching. CART devices are easy to realize, tailor, and post-functionalize. A photo-polymerizable phase-separating resin is used to 3D-print porous carriers that are then infused with ferrofluid to make them magnetically responsive, enabling untethered cargo manipulation on both solid and liquid substrates. Using CART, various cargos can be remotely moved, rotated/mixed, inverted, and lifted, further facilitating interaction between two carriers for transferring, merging, and tunably splitting cargo. Overall, CART advances microcargo manipulation by decoupling cargo from the substrate and leveraging magnetic responsiveness for untethered, versatile control across different environments, opening up new actuation-modalities.

1. Introduction

The miniaturization of experiments facilitates accelerated research in fields such as drug discovery, diagnostics, biotechnology, analytical chemistry, and sensors, among many others. One example is the use of microdroplet environments, which can be realized via surface arrays[1] or droplet microfluidics.[2] While surface arrays facilitate individual droplet access, their immobility constrains the dynamic manipulation of these microenvironments. To maintain experimental flexibility similar to that of larger classical experiments, substrates and droplets have been functionalized to stimulate droplet actuation and manipulation; allowing them to move, merge, mix, and split.[3] Some methods provide pre-determined droplet actuation, such as surfaces with built-in wettability anisotropy,[4] while others allow for reprogrammable droplet actuation. Different stimuli utilized for the latter include electricity,[5,6] light,[7,8] and magnetism.[9] Currently, electrowetting is the most advanced automated liquid manipulation strategy, but requires a substrate prepatterned with electrodes, while light-stimulation allows high-resolution spatiotemporal control, but still offers comparatively fewer actuation modes.[10,11] Magnetism has the advantage of providing flexible substrate choice and untethered actuation without the need for an optically transparent system.

The methods of magnetic actuation can be divided into three categories. The first strategy involves adding functional materials into the cargo. For instance, Li et al.[12] added two magnetic steel beads to a droplet on a hydrophobic substrate, which allowed the droplet to be dragged around as surface tension inhibited its release. Depending on the geometry and bead velocity, the droplet is split, mixed, or the beads could be released. This method can transport both water and gas in immiscible fluids. The second strategy involves modifying the substrate to enable cargo movement. Zhang et al.[13] demonstrated that placing a water droplet on a substrate covered with oil-based ferrofluid results in the formation of a capillary-force induced ferrofluid wetting ridge around the droplet. The wetting ridge and the droplet can be moved on the substrate using a magnet, allowing for the transportation of both liquid droplets and solid particles. The final strategy involves enclosing the cargo in an actuatable "package". Jiang et al.[14] developed a magnetic Janus origami robot that wraps around droplets using capillary forces. This robot can be rolled across the substrate or squeezed to release the droplet

N. K. Mandsberg, J. A. Serna, P. A. Levkin
Karlsruhe Institute of Technology (KIT)
Institute of Biological and Chemical Systems – Functional Molecular Systems (IBCS-FMS)
Kaiserstraße 12, 76131 Karlsruhe, Germany
E-mail: nikolaj.mandsberg@kit.edu; levkin@kit.edu
P. A. Levkin
Karlsruhe Institute of Technology (KIT), Institute of Organic Chemistry (IOC)
Kaiserstraße 12, 76131 Karlsruhe, Germany
The ORCID identification number(s) for the author(s) of this article can be found under https://doi.org/10.1002/adfm.202406635

DOI: 10.1002/adfm.202406635

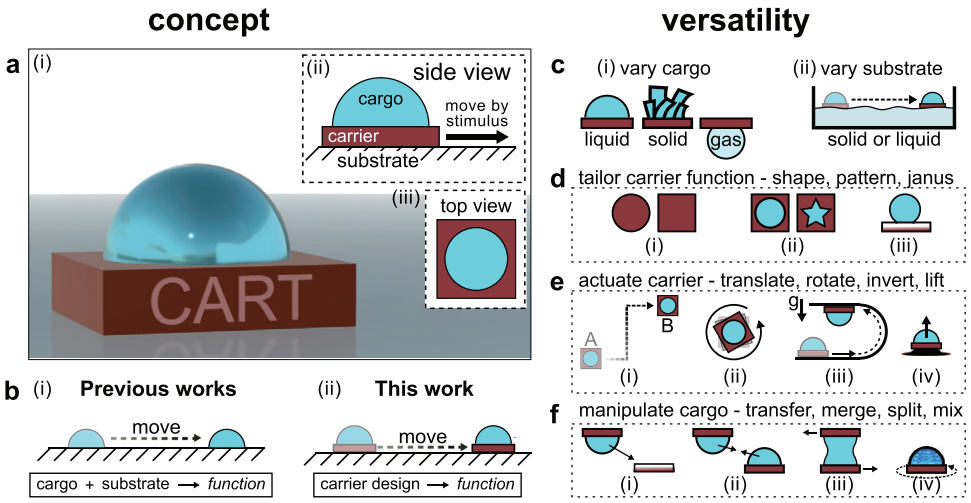

Figure 1. Concept of Carrier-based Actuatable and Reprogrammable Transport (CART), an approach for manipulating and transporting microcargo on substrates. a) CART uses a magnetically actuatable carrier intermediate between the cargo and the substrate. b) The combination of substrate and cargo no longer is responsible for the functionality; rather, the functionality is integrated into the carrier thereby decoupling cargo and substrate choices. This gives, c) high versatility in both (i) cargo choice (liquid, solid, gas) and (ii) substrate choice (solid or liquid). d) Carrier properties can be tailored via (i) shape, (ii) patterning, and (iii) differences in top and bottom properties ("Janus" properties). e) Carrier actuation includes untethered (i) translation, (ii) rotation, (iii) inversion, and (iv) lifting. f) A multi-carrier system permits additional manipulation of the cargo, such as (i) transfer, (ii) merging, (iii) splitting, and (iv) mixing, making CART a powerful tool with potential for diverse application fields.

back onto the substrate. This method can be scaled down to manipulate even nanoliter-sized droplets.

Although a plethora of actuation methods exploiting different strategies have been developed, they generally share a set of challenges: reducing droplet-substrate friction is crucial for enabling movement; chemical traces can lead to inter-droplet contamination; droplet-substrate compatibility requirements constrains both substrate choice and droplet material. Moreover, it is important to manipulate not only liquid, but also solid and gas cargo; collectively referred to as *"cargo"* throughout the manuscript. We realized that many of the aforementioned challenges arise from sharing the same substrate, which limits compatibility, reduces customizability, and risks cargo contamination.

Here we introduce the concept of CART: Carrier-based Actuatable and Reprogrammable Transport. CART is a simple strategy for enabling miniaturized transport and manipulation of liquids and solids on both solid and liquid substrates. Similar to a shopping cart, a "carrier" is inserted between the substrate and the cargo (**Figure 1a**). The transporting functionality is now shifted from the cargo to the carrier, which can be used universally for both different cargoes and different substrates. The carrier introduces both an additional interface and a spatially unconstrained bulk material, which together eliminate the common challenges and enable new opportunities. The bulk of the carrier can be functionalized to respond to magnetic stimulation, while the extra interface eliminates the need for cargo-substrate matching. This provides freedom in cargo selection without any changes to the substrate. The elimination of the substrate-cargo interface also removes the need to minimize cargo-substrate friction, which further broadens the application space of CART. This paper demonstrates the ease of realizing the CART system, its magnetic functionalization for untethered actuation and cargo manipulation, and its versatility. The aim is to inspire researchers to use the system directly and to further develop its capacities.

2. Results

The CART system consists of a substrate, a carrier, and a cargo, as depicted in Figure 1a. Unlike previous studies, the cargo actuation is decoupled from the substrate choice by inserting a carrier (Figure 1b). This has three significant advantages. First, it increases versatility in cargo and substrate choice by eliminating the need for cargo-substrate matching, i.e., the substrate can be generalized to different cargoes (Figure 1c). Second, each cargo has a "local substrate", which can be customized for desired cargo-carrier interactions (see Figure 1d). Third, by eliminating the cargo-substrate interface, we not only remove the need to minimize friction, but even turn friction into an advantage. This is because high friction facilitates high-speed movement of the cargo without slipping off the carrier.

The CART system requires a stimuli-responsive carrier for cargo actuation. In this work, magnetism is utilized as the stimulus. Magnetic ferrofluid is added to the carrier material, allowing it to be moved by a nearby magnet; such as one beneath the substrate. Actuation modes include translating the cargo from one point to another by translating the magnet (Figure 1e-i), rotating the cargo by rotating the magnet (Figure 1e-ii), turning both carrier and cargo upside-down by moving it along a curved substrate (Figure 1e-iii), and lifting the cargo by increasing the magnetic field (B-field) strength (Figure 1e-iv). The ability to invert the carrier opens up new possibilities in multi-carrier systems, such as cargo transfer (Figure 1f-i), cargo merging (Figure 1f-ii), and cargo splitting (Figure 1f-iii), while the opportunity for rotation enables mixing (Figure 1f-iv). Overall, the CART system supports both typical and atypical modes of untethered movement and actuation.

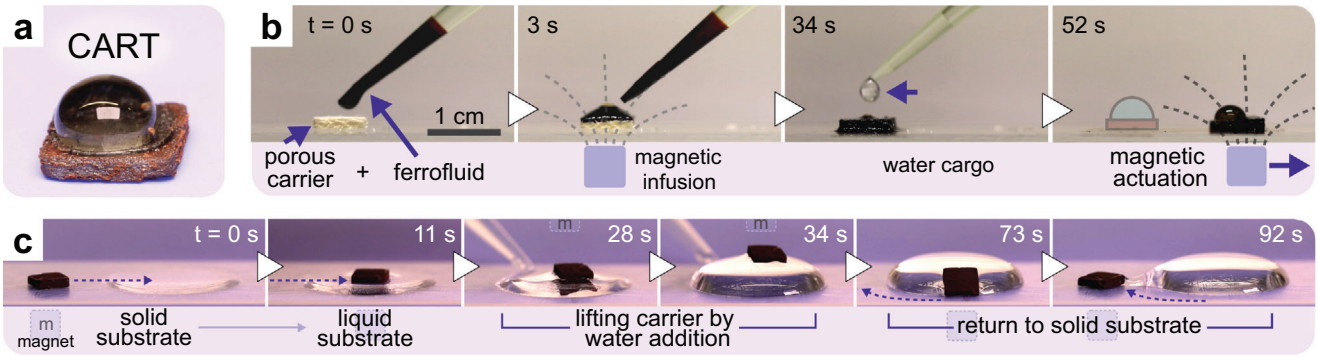

Figure 2. Simple realization of CART. a) Photo of a basic CART system (solid substrate, magnetic carrier, and water-based cargo). b) This specific carrier type is created by infusing ferrofluid into a porous material, thereby making it magnetically responsive for untethered cargo transport. c) CART has amphibian characteristics: Photo sequence of the carrier being moved from a dry to a wet substrate, then lifted by inflating a water droplet, and finally returned from liquid substrate to its home position on the solid substrate.

Setting up and using a basic CART is simple. An example of a carrier with cargo (≈20 µL water) is presented in **Figure 2a**. The raw carrier is produced using Digital Light Processing (DLP) 3D printing and a photopolymerization-induced phase separating resin.[15] (Table S1, Supporting Information details the recipe, adopted directly from Mandsberg et al.[16]). This allows for the creation of carriers with digitally defined macroscopic geometry (Figure S1, Supporting Information) and sub-micrometer porosity that are compatible with solid, liquid, and gaseous cargo (Figure S2, Supporting Information). The carrier's dark appearance is due to the infusion with ferrofluid.

Starting from a porous carrier (see ref. [16] for morphological details), the preparation of a functional CART takes less than one minute. The process of infusing the carrier with an oil-based ferrofluid to enable its magnetic actuation with a $5 \times 5 \times 5$ mm^3 neodymium magnet is shown in Figure 2b. The magnetization of the porous carrier takes less than 30 s, limited only by the time scale of oil wicking (Movie S1, Supporting Information). On high-friction solid substrates, the oil can serve a dual purpose, acting both as a means of actuation and as a lubricant.[17] For other substrates, the oil may be left to evaporate, resulting in a dry magnetic carrier, which eliminates substrate contamination and trail creation as well as the risk of contaminating cargo with the ferrofluid. It is noted that careful selection of the ferrofluid type is necessary to eliminate cargo contamination completely.

Figure 2c demonstrates the movement of such dry magnetic carrier on a glass slide with a chemical wettability pattern (Movie S2, Supporting Information). As a magnet beneath the substrate moves to the right, the magnetic carrier mimics its motion, shifting its position from a dry hydrophobic region (0 s) to a wetted hydrophilic region (11 s). Repositioning the magnet to above the wetted zone can create a stabilizing force field, effectively balancing magnetic and gravitational forces on the carrier. As a result, the carrier can be lifted by inflating a droplet beneath it (28 s and 34 s). The stabilizing field is crucial for balancing the carrier on this highly curved liquid substrate. When floating on this droplet, the carrier experiences extremely low friction, which, as later shown, enables novel functionalities, such as rotation. Finally, the stabilizing top magnet can be removed to release the CART, making it slide to the edge of the drop (73 s). At this point, a magnetic field from the bottom can be applied to return the carrier to its original position (92 s).

To unlock additional functionalities of the carrier, one approach is to differentiate its top and bottom surface properties; here coined "*Janus carrier*" or "*jCART*". **Figure 3a-i** shows a basic implementation of jCART, which involves attaching a silicon (Si) chip to the top of a dry magnetic carrier using double-sided tape (total weight ≈0.17 g). The jCART supports liquid (Figure 3a-ii), solid (Figure 3a-iii), and gaseous (Figure 3a-iv) cargo. The first two are demonstrated on solid substrates, while the latter floats atop a water reservoir on its Si-chip belly. Experiments indicated that pinning of water at the Si chip edges can encapsulate gaseous cargo in a liquid layer for transfer between reservoirs, as seen in Movie S3 (Supporting Information). The Si chip also provides an interface that can be customized for desired cargo interactions and serves as a "*function barrier*", preventing the actuation region from interfering with the cargo by constituting a non-permeable barrier between the two (Figure 3a-v). One type of Si chip used in this study had a 3 mm circular hydrophilic center spot in a hydrophobic matrix (Figure 3a-vi), and with nanoscale roughness across the entire surface to enhance the chemically-induced wettability contrast (Figure 3a-vii; Table S2, Supporting Information). The center region is highly pinning, while the surrounding area has low pinning. This allows water-cargo to strongly adhere, enabling high-speed carrier movement without the cargo slippage, as later demonstrated.

The jCART adeptly transports cargo across various solid surfaces. The video frame montage in Figure 3b showcases this operational versatility by transporting solid cargo (weight ≈11 mg) across three material zones. Starting on a hydrophobic-hydrophilic glass slide, passing through wetted zones, transitioning to a zone with high roughness (backside of tape), and finally moving onto a stretched nitrile glove (Movie S4, Supporting Information). While the carrier exhibits smooth movement on both dry and wetted nitrile, it exhibits moderate stick-slip behavior on glass and tape. This variance in performance suggests that matching the carrier's bottom with the substrate characteristics is crucial for ensuring smooth movement across different surfaces.

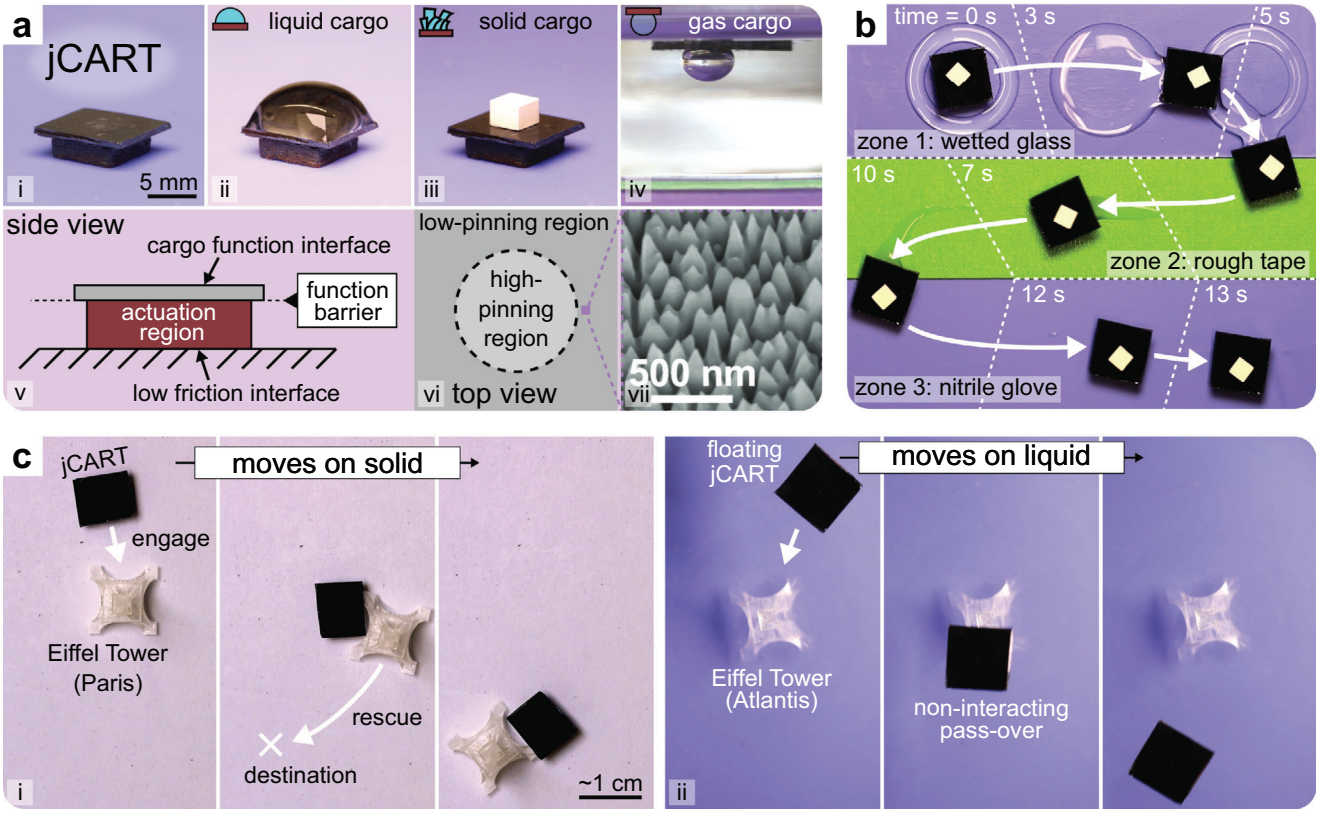

Figure 3. jCART's (Janus-CART) adaptability with various cargoes and substrates. a) Advanced jCART system (i) photographed with diverse cargo types: (ii) liquid, (iii) solid, and (iv) gas. The jCART comprises an (v) actuation region and a functionalized top-part, such as a (vi-vii) nanostructured silicon chip with a highly water pinning hydrophilic circular region surrounded by a superhydrophobic barrier. b) Video frame montage of continuous jCART actuation across diverse solid surfaces (dry and wet glass, textured tape, and nitrile glove). c) Sequential images demonstrate the jCART (i) rescuing a mini-Eiffel Tower model on a solid surface, and (ii) operating non-interactively on a liquid substrate, hovering over the submerged model.

The magnetic force is well-balanced, enabling jCART actuation without increasing friction to the point of inhibited mobility. This balanced force also enables the carrier to manipulate objects that are not loaded onto it, but can be pushed around, see Figure 3c-i. While the demonstration here is a rescue mission of the Eiffel Tower, such repositioning of laboratory objects (e.g., optical elements) could make CART useful for advancing laboratory automation. Furthermore, the lightweight nature of the carrier allows it to float on water; as evidenced by the ability to perform a non-interacting pass-over of a submerged Eiffel Tower, see Figure 3c-ii. CARTs amphibious properties (demonstrated in Figure 2c) enable utilization of both solid and liquid substrates, leveraging the unique advantages of each (Figure S3 and Movie S5, Supporting Information).

Liquid cargo can also be transported along curved substrates; even be turned upside-down. In **Figure** 4a, a plastic sheet has been bent to form a half loop, along which a carrier with water-cargo is moved horizontally, vertically, and in an inverted position (Figure S4 and Movie S6, Supporting Information). The latter is here made possible by capillary adhesion between the water cargo and oil-infused carrier. In this case, the oil led to cloaking of the water-cargo, but it can be uncloaked by changing the type of oil.[18] or circumvented using a jCART (design in Figure 3a-vi).

The maximum water-cargo volume depends on several parameters, such as carrier design and orientation. Using side-view imaging on a drop shape analyzer, we determined the maximum cargo volume for circular carriers of diameters $d = 3$ and 8 mm (Figure 4b). When the carrier is oriented horizontally, the apparent advancing contact angle at the carrier edge ($\theta_A = 154 \pm 1$, $n = 6$) limited the maximum cargo volume, making it highly dependent on carrier diameter (41 µL for d = 3 mm and 243 µL for d = 8 mm) (Figure S5 and Table S2, Supporting Information). In this orientation, gravity is largely balanced by a normal force from the carrier; which will expectedly make $V_{max} \approx d^3$ for spherical cargo and $V_{max} \approx d^2$ for puddle cargo.[19] On the other hand, in the vertical (Figure S6, Supporting Information) and inverted (Figure S7, Supporting Information) orientation, gravity did compete with cargo-carrier adhesion, significantly reducing V_{max} to 13–17 µL and 34–41 µL, respectively. For the investigated diameters and both directions, V_{max} is reached prior to full surface coverage of the carrier, resulting in limited interaction between the carrier's perimeter/edge and cargo. As a consequence, V_{max} is largely independent of d. Besides the carrier design and orientation, the properties of the liquid cargo such as surface tension and density are expected to significantly affect V_{max}; limitations are closely related to those of maximum puddle height.[19] and pendant drop size.[20] Finally, it is important to note that V_{max} is likely to be lower for dynamic carriers compared to the static carriers evaluated in this study due to kinematic effects on the liquid-cargo shape. However, if necessary for

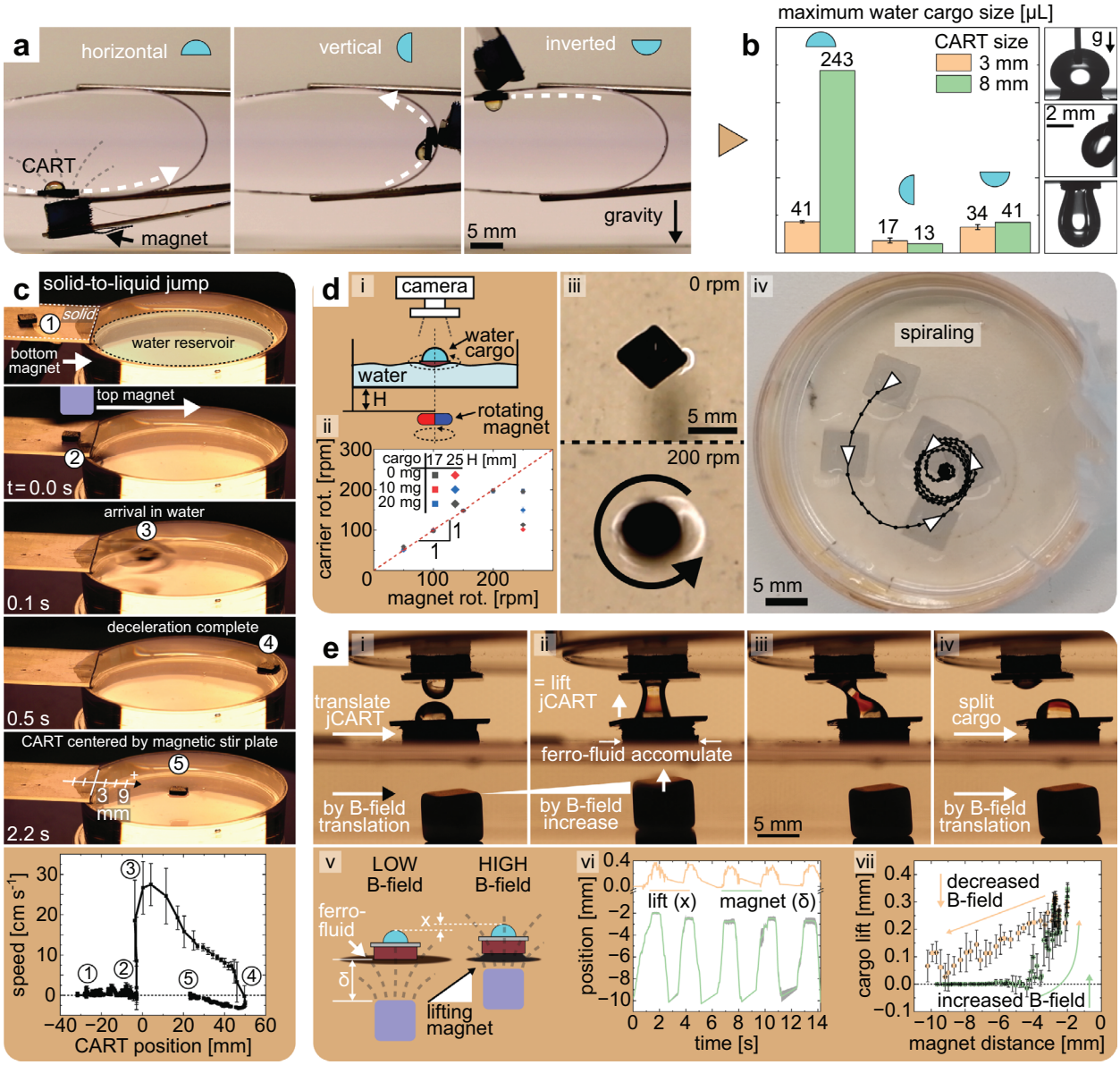

Figure 4. Carrier actuation. a) Magnetic attraction facilitates complete carrier inversion along a curved substrate. b) Carrier size and orientation affect water cargo capacity for 3 mm and 8 mm circular carriers, with insets showing maximum loads for the 3 mm carrier (n = 3). c) (1-5) Sling-shot maneuver-inspired transition of CART from solid to liquid substrates, with (bottom) quantified carrier speed. d) Ultra-low friction enables rotation and spiraling on liquid substrates: (i) setup, (ii) angular speed operational range, and (iii) photos at rotational extremes (0 and 200 rpm). (iv) Spiraling motion sequence. e) Cargo merging demonstrated through magnetic lift, highlighting the option for non-lateral actuation: (i) separated jCARTs, (ii) lift via magnetic field-induced ferrofluid accumulation, (iii-iv) cargo splitting, (v) lifting mechanism schematic, (vi) lifting-reversibility over five cycles, and (vii) magnet distance versus lift relationship (n = 5).

a specific application, V_{max} may be increased by optimizing the carrier design.

The choice of substrate (solid or liquid), depends on the carrier task. By developing additional ways to move between the two, the usefulness of CARTs is expanded. Figure 4c shows the carrier jumping from a solid substrate (a glass slide) to a water-filled Petri dish. On solid substrates, a magnet beneath moves the carrier, but top actuation fails as the magnetic force prematurely pulls the carrier toward it, preventing smooth lateral movement. However, inspired by the slingshot maneuver used in space exploration, where a body moving relative to a radial force field is attracted yet escapes it, we transferred a carrier from solid to liquid substrate. By performing a high-speed magnet pass-by, the carrier is moved without being fully captured by the magnet's pull. Figure 4c-top displays the entire process, which involves the initial movement by a bottom magnet, acceleration by a top magnet passing by in high speed, and stabilization in the center of the Petri dish by a magnetic stirrer positioned below (Movie S7, Supporting Information). During transfer, the carrier reached a maximum speed of ≈20–30 cm s^{-1},

requiring ≈20–40 milliseconds for the transition (see Figure 4c-bottom).

On the liquid substate, the carrier (density ≈1.2 g cm^{-3}) can be rotated at controlled angular speeds using a standard magnetic stirrer (see Figure 4d-i). The system exhibits a one-to-one relationship between the angular speed of the magnetic actuator and the actuated carrier from 0 to 200 rpm (Figure 4d-ii). However, beyond 200 rpm, the carrier cannot keep up, presumably due to viscous drag from the reservoir (Figure S8, Supporting Information). This result is independent of distance to actuator in the range 17–25 mm and cargo weights up to the tested maximum of 20 mg. Photos in Figure 4d-iii illustrate the minimum (0 rpm) and maximum (200 rpm) angular speeds allowed by this setup (Movie S8, Supporting Information). The operational range is influenced by factors such as magnetic field strength, magnetization and geometry of the carrier, cargo properties, and setup geometry. Optimizing these parameters may extend the operational range, but that task is beyond the scope of this work. Another feature of the liquid substrate's low friction is that inertia can overcome friction, leading to a spiraling motion of the carrier on a magnetic stirrer, as illustrated in Figure 4d-iv and Movie S9 (Supporting Information). This motion results from the rotating magnet beneath, which applies both radial and tangential forces, guiding the carrier toward the rotation axis. Once at the center, the carrier continuous to rotate around its own axis.

CART is not limited to lateral motion, but can also move orthogonal to the substrate in the presence of excess ferrofluid (Movie S10, Supporting Information). Initially, the ferrofluid serves as a lubricant, enabling easy sideways movement under a mild magnetic influence (see Figure 4e-i). However, approaching the magnet to the substrate intensifies the magnetic field, causing the ferrofluid to accumulate beneath the jCART. With the ferrofluid under the jCART, the jCART is lifted, in this case causing its cargo to coalesce with another liquid cargo positioned above (Figure 4e-ii). Lateral displacement of the magnet can separate the coalesced liquid cargoes back into two distinct volumes (Figure 4e-iii/iv); cargo splitting will be explored in more detail later. This lifting process is reversible; withdrawing the magnet diminishes the magnetic field, allowing the ferrofluid to relax and settle back into its spread state, thereby lowering the jCART. Figure 4e-v shows five cycles of lifting and lowering, while Figure 4e-vi details the correlation between the proximity of the magnet and the elevation of the cargo. In our setup, lifting starts at a magnet distance of ≈4 mm, with a peak elevation of 0.35 mm. As is evident, the return to the original elevation follows a different dynamic compared to the lifting. This indicates that the relaxation time of the ferrofluid, rather than the position of the magnet, governs this stage of the cycle. The opportunity for substrate orthogonal cargo movement makes it easier to selectively avoid and merge with specific cargoes among a myriad of cargoes.

Theoretical exploration of magnetically responsive fluids deepens our understanding of magnetic lifting. As the magnetic field strength and its vertical gradient increase, a ferrofluid droplet reshapes, achieving equilibrium by balancing gravitational, magnetic, and surface energies.[21] The field strength and droplet deformation are interdependent, complicating the calculation of magnetic energy, and the determination of the equilibrium shape.[22] Generally, as the magnetic field strengthens, the ferrofluid droplet elongates along the field direction, with a nonlinear relationship between field strength and droplet height.[23] Above a critical field strength, the droplet undergoes stepwise division, producing smaller daughter droplets that furthermore self-assembles into a field-dependent pattern.[24] In carrier lifting, as the magnet approaches the substrate and intensifies the field, the ferrofluid adjusts to a taller equilibrium shape in milliseconds, enabling carrier lifting with minimal latency. Conversely, reducing the field causes the ferrofluid to spread, with nanoscale interactions complicating the behavior and making relaxation time estimation challenging.[21] This complicates the estimation of relaxation times, although studies indicate that ferrofluid spreading on hydrophilic substrates at zero field typically occurs within seconds.[25] Ongoing research continues to explore ferrofluids' dynamic behavior and their utility in manipulating both solid and liquid object.[26,27]

The interaction between multiple cargoes is crucial for the usefulness of CART. Unfortunately, one drawback of using carriers is the presence of "dead zones" near the edges of the carriers, which generally prevents physical contact between cargoes positioned on separate carriers. However, this problem can be easily solved using CART's "property of inversion". By moving carrier "A" along a curved substrate (as was shown in Figure 4a) to contact carrier "B" from above, the "dead zone" is circumvented – this action is somewhat analogous to curving a 2D substrate-space to create a worm-hole-like-connection of two spatially separated locations. Using this unique technique for combinations of the basic CART and the jCART, water-cargoes are successfully 1) transferred from a basic carrier to a jCART (**Figure 5**a), 2) merged from different carriers onto a jCART (Figure 5b), and 3) split onto two separate jCARTs (Figure 5c). In certain instances, the inversion approach may be employed to circumvent the "dead zones" for gas and solid cargoes. It is worth noting that side-by-side merging may also be possible through further carrier optimization or the addition of constraints on liquid cargo volumes. A proof-of-concept demonstration can be found in Figure S9 (Supporting Information).

Moreover, we discovered a tunable method to split water-cargo into two volumes, V, of unequal size. By changing the carrier separation speed, the splitting ratio (V_{top}/V_{bottom}) could be adjusted by up to a factor of two (Figure 5d,e; Figure S10, Supporting Information). This ability is akin to that of dip-coating processes, wherein film thickness for chemically homogeneous substrates,[28] and droplet height for chemically heterogeneous substrates.[29] have been found to depend on withdrawal velocity. In our scenario, unlike the well-known dip-coating experiment, the reservoir volume is no longer effectively infinite but instead comparable to the droplet formed. In our experiment, the upper carrier is dynamic (emulating the dip-coated substrate), while the lower is static (emulating the reservoir). At low speeds, the size of the upper dynamic droplet increases with increasing separation speed. The splitting ratio increases until the speed reaches 10 to 17 cm $^{-1}$s, and subsequently decreases as the speed is increased further. This behavior is also consistent with dip-coating of substrates, which experience a transition from a low-speed to a high-speed regime at ≈16 cm s^{-1}, when the Froude number, the ratio of flow inertia to gravity, reaches unity.[30]

The potential for 100% transfer efficiency, equivalent to a splitting ratio of 0, is contingent on the precise wettability of the carrier surface. While the high adhesion between droplet

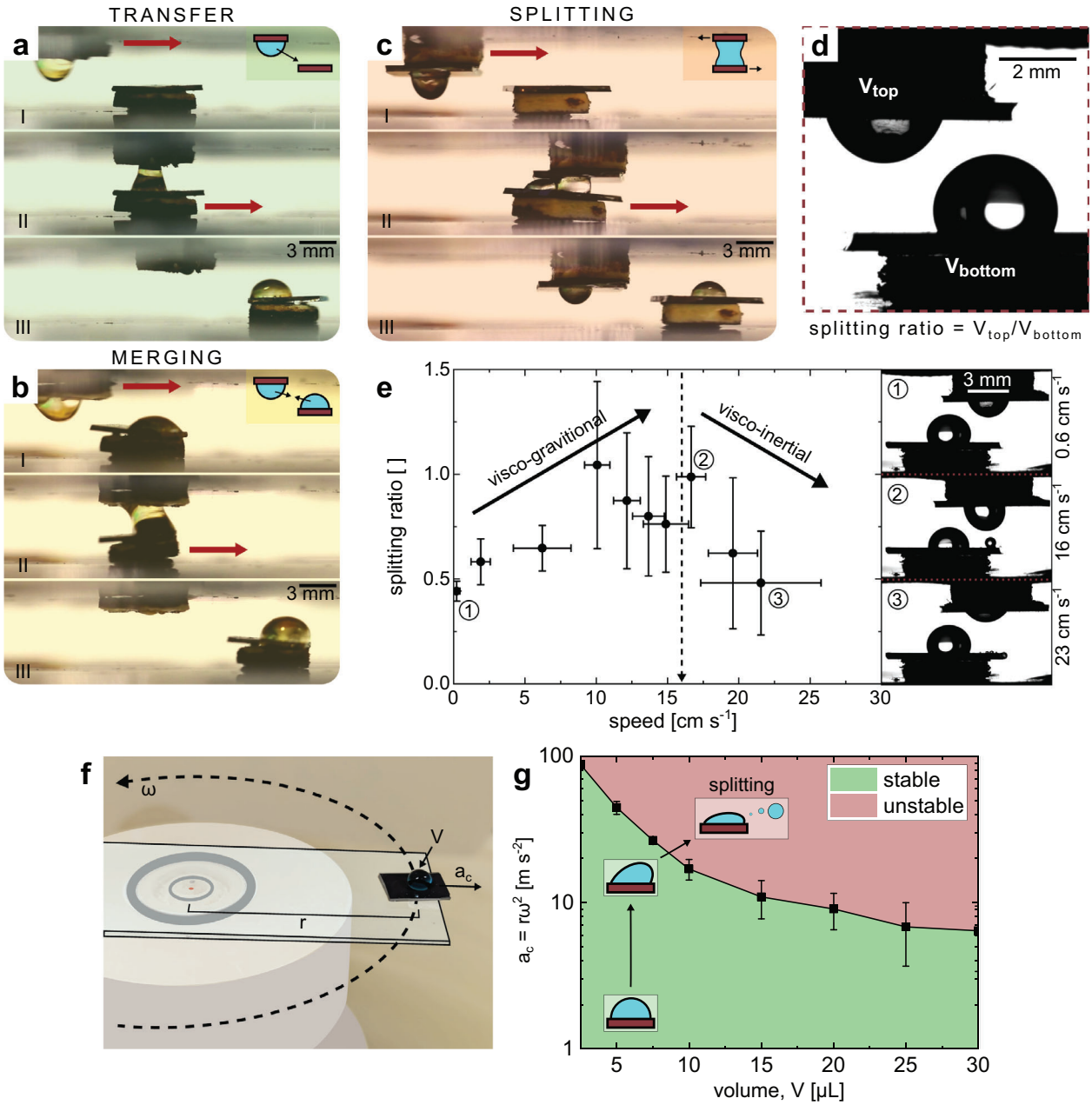

Figure 5. Liquid cargo manipulation in a two-carrier system. A two-carrier system with one horizontal and one inverted carrier enables cargo manipulation: a) transfer, b) merge, and c) split. d,e) By changing the speed of carrier separation, the splitting ratio can be tuned. Inserts show splitting for speeds of 0.6, 16, and 23 cm s^{-1} (n = 5). f, Experimental setup to determine the limit of stable transport of liquid cargo. g, Phase diagram showing the stable/unstable transport of water cargo with a jCART (3 mm hydrophilic spot) for variation of (dyed) water cargo volume, V, and carrier acceleration, a_c (n = 3 device replicates).

and carrier facilitates the stability of single-carrier droplet transport, it also creates non-slip conditions with a viscous boundary layer, precluding the possibility of 100% transfer efficiency. However, building on previous work in droplet manipulation, which has predominantly relied on hydrophobic or superhydrophobic substrates to achieve precision and controllability via nano- or microstructuring,[31,32] one could add controllable wettability regulation to the top surface of the carrier to potentially mitigate this limitation. One could also consider adding magneto-orthogonal stimulus-responsive wettability to facilitate on-demand cargo capture/release, such as metal oxide thin films with light-induced hydrophilicity.[33,34] to create a temporary wettability asymmetry between the two otherwise identical jCARTs.

As mentioned, the carrier-cargo friction can also be advantageous, because the strong adhesion facilitates high-speed movement of the carrier with its cargo slipping off. By utilizing a rotational setup (see Figure 5f), the maximum acceleration of the

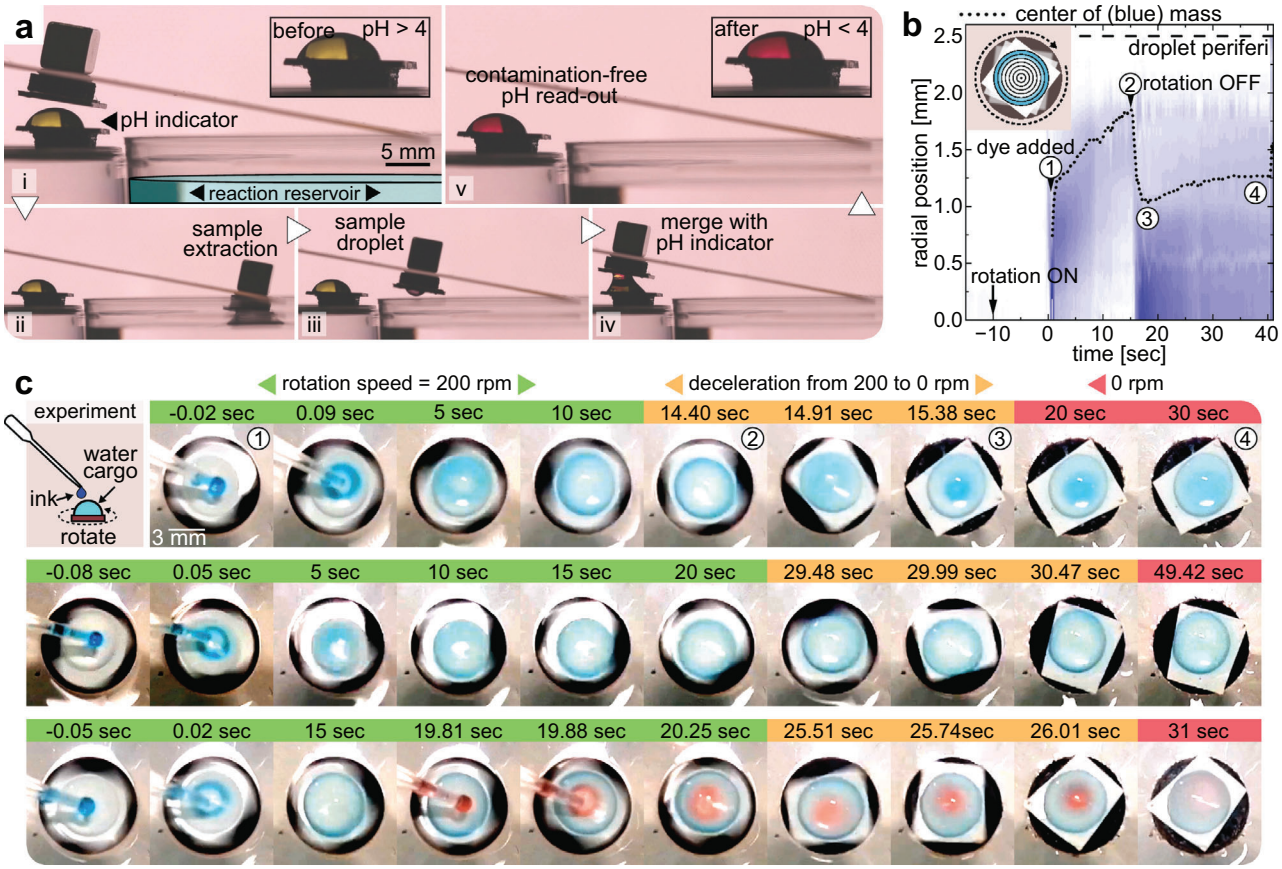

Figure 6. Reservoir Sampling and Tea Leaf Effect. a) pH measurement application. (i) A CART is prepared with a pH-sensitive indicator cargo. (ii) Non-contaminating sample extraction from reaction reservoir with an inverted jCART. (iii) Extracted sample. (iv) Merging sample with the indicator cargo results in (v) a colorimetric change, indicating the acidity level of the reservoir. b) Tea leaf effect quantification: Heatmap visualizing distribution of blue dye over time in rotated micro-droplet (analysis of C – top row). c) Visualization of Tea Leaf Effect. A water cargo carrier is rotated, causing added dye to migrate to the droplet triple line. Subsequently, deceleration induces a secondary flow that can centralize the dye. (top row) Video frame sequence demonstrates the effect, visible only when deceleration precedes a critical timing. (middle row) Delaying deceleration beyond this point leaves the dye at the droplet's edge. (bottom row) Exploiting this timing, we spatially separate two dyes by introducing them at intervals governed by the critical timing.

jCART is determined. A biphilic chip (3 mm hydrophilic spot size), loaded with different water cargo volumes, is mounted on a spin-coater at a distance from the rotational axis of $r = 18$ to 32 mm, and spun at increasingly higher rotational speeds, ω. The ramping rate, α, is 10 to 20 rpm s^{-1}. The rotational speed is increased until liquid cargo leaves the carrier, which marks the threshold for maximum acceleration. Equation (1) shows the calculation of the total linear acceleration, a_{total}, by combining the centripetal (radial) acceleration, a_c, and the tangential acceleration, a_t.

$$a_{total} = \sqrt{a_c^2 + a_t^2} = \sqrt{(r\omega^2)^2 + (r\alpha)^2} \quad (1)$$

For the selected rotational accelerations of 10 to 20 rpm s^{-1}, the tangential acceleration is $\lesssim 0.04$ m s^{-2}, making it negligible compared to the centripetal acceleration. Therefore, the total acceleration can be described by Equation (2) within a 1% error.

$$a_{total} \approx a_c = r\omega^2 \quad (2)$$

Figure 5g presents the phase diagram of stable and unstable combinations of cargo volume and acceleration speed. For all investigated volumes, only a fraction of the cargo departed, leaving behind cargo residues on the hydrophilic spot. In some cases, the threshold for stable cargo approaches 10G, which makes using a rotational system highly advantageous, as a linear acceleration system would require meters of travel distances, which is often beyond what is experimentally practical.

Another feature of the jCART is the possibility to extract a liquid sample from a larger reaction reservoir for monitoring (Movie S11, Supporting Information). For demonstration purposes, we prepared a carrier with a 50 µL pH indicator droplet, as shown in **Figure 6**a-i. Positioned above is an inverted empty carrier. By moving this inverted carrier on an inclined substrate, the reaction reservoir can be contacted (Figure 6a-ii). The hydrophilic region of the jCART silicon chip wets upon contact, and as the jCART is returned, it extracts a sample droplet (Figure 6a-iii). Bringing the inverted jCART and pH indicator jCART together allows for the mixing of the sample cargo with the pH indicator cargo (see Figure 6a-iv). Because the reaction reservoir contained a solution of diluted hydrochloric acid pH 2, mixing

triggers a color change, revealing the low pH of the reservoir; all without contaminating it during the characterization process (Figure 6a-v). It is worth noting that the indicator drop is here pipetted to the carrier, although it could have been extracted and inverted from a reservoir to conduct the entire process solely with the CART system. This method of extracting small samples enables both monitoring of reactions and loading jCARTs with reactive cargoes for in-line synthesis and product characterization. Significantly, the CART system could potentially be adapted for high-throughput applications by managing multiple droplets simultaneously. Enhancing magnetic field confinement and integrating with Droplet Micro Array technology[35] could, respectively, allow multiple carriers to handle tens of droplets each, significantly boosting throughput and operational flexibility for parallel processing in scientific and industrial environments.

Moreover, there is potential for the CART system to be expanded for high-throughput applications by enabling the simultaneous management of multiple droplets. This could be achieved by confining the magnetic field to reduce repulsion between different "driving magnets". Additionally, by integrating CART with Droplet Micro Array technology, each carrier could potentially handle not just one, but tens of droplets. This could significantly increase throughput and flexibility, opening possibilities for parallel processing and enhanced efficiency in scientific and industrial settings.

Finally, unique to the CART system is the ability to rotate the cargo, which we hypothesized could provide an opportunity to manipulate the internal flow of liquid cargo (Movie S12, Supporting Information). In Figure 6b, a 2 µL dyed droplet is added to an already rotating 20 µL droplet (200 rpm). Over time, the dye migrates to the edges of the rotating droplet. Very interestingly, if the droplet rotation is stopped within 15 seconds of adding the dye, the dye "jumps" back to the center before finally homogenizing the droplet by diffusion (Figure 6b,c – top row). This phenomenon may be caused by the tea leaf paradox,[36] first described by A. Einstein. In this situation, the primary flow is the vortex flow. However, in the transient phase of the droplet rotation, a secondary flow is created, caused by the boundary layer induced by the no-slip condition, which gives rise to a pressure gradient-induced flow toward the center. On the contrary, if the deceleration occurs after this critical time point, the dye remains at the edge even after the rotation is stopped (Figure 6c – middle row). It is hypothesized that the cause of this phenomenon is dye migration into flow-inhibiting pockets near the triple-line of the liquid cargo. In Figure 6c – bottom row, the two behaviors are combined in a single liquid cargo by adding dyes at different time points; first blue, then red, each corresponding to one of the two regimes. The outcome is a spatial reseparation of the two dyes.

3. Conclusion

The CART system is developed to address longstanding challenges in microcargo manipulation. Unlike traditional methods that rely on specific substrate-cargo interactions and friction reduction, CART uses a simple magnetic carrier to physically separate the cargo from the substrate. This allows for untethered and controlled manipulation of solid and liquid cargo across both solid and liquid substrates, incorporating amphibious properties to exploit the unique benefits of each. This multi-cargo, multi-substrate transport differentiates CART from previous actuation methods. Moreover, eliminating the need for cargo-substrate matching allows individual carriers to be tailored to specific cargoes and opens the possibility to use a generalized substrate to manipulate multiple types of cargo simultaneously. This not only enables diverse cargo confinement but also tailored interaction between the carrier and cargo, including preparing carriers for liquid cargo content analysis.

One drawback of the carrier-based system is its finite area, which limits the maximum cargo size, and its "dead zone" (i.e., the space between the droplet and the edge of the carrier), which prevents side-by-side merging. The merging issue is resolved by rethinking how objects can be approached on a 2D substrate; by folding the 2D substrate plane, distant locations are brought into proximity and cargo easily merged from the third dimension. This solution may inspire novel ways of rethinking and circumventing typical 2D substrate constraints. Another approach to resolve the issues could be refinements of the carrier design, by which it is expected that CART could be made modular, allowing for dynamic adjustment of carrier size and facilitating side-by-side merging of liquid cargo via carrier asymmetries. Similarly, optimizing the carrier rotation setup could increase the maximum angular speed beyond 200 rpm, thus unlocking on-demand reversible particle centrifugation.[37] This ability could be used to temporarily open an optical window for scatter-free reaction monitoring: As the carriers are 3D printed, they could be prepared with a hole in the center, allowing for transmission measurements as well as be made both smaller and larger. Another property worth noting is that rotation starts at the cargo-carrier interface, propagating through the cargo, which facilitates a laminar flow affecting the entire cargo for controllably modulating the internal flow of this micro-sized droplet. In particular, the features mentioned above could be utilized for colloidal assembly.

Future research may aim to optimize the CART system for greater efficiency and broader applications. This could involve developing carrier designs to accommodate additional functionality, as well as integrating stimuli-responsive materials to interact with the cargo. These improvements would unlock even more complex manipulation tasks and expand the utility of CART in various scientific and medical fields.

4. Experimental Section

Detailed materials and methods can be found in the SI file, Supplementary Text.

Supporting Information

Supporting Information is available from the Wiley Online Library or from the author.

Acknowledgements

The authors thank Joaquin Urrutia (KIT) for 3D illustration, Mariia Kuzina (KIT) for discussion of Figure 1, and Anna Shneidman (Harvard University) for the discussion on the general concept of CART. DTU Nanolab (Technical University of Denmark) is thanked for contributing with repurposed silicon samples prepared in their fabrication facilities in 2019.

Funding: P.A.L. thanks DFG (Heisenbergprofessur; 406 232 485 and LE 2936/9-1) for the financial support. The authors thank the Excellence Cluster "3D Matter Made to Order" (2082/1-390761711) and the Carl Zeiss Foundation for financial support. J.A.S. acknowledge funding from German Academic Exchange Service (DAAD). N.K.M was funded by an Internationalisation Fellowship from the Carlsberg Foundation (CF21-0614).

Open access funding enabled and organized by Projekt DEAL.

Conflict of Interest

The authors declare no conflict of interest.

Author Contributions

As per the CReDiT terminology, N.K.M. performed conceptualization, methodology, software, Validation, formal analysis, investigation, writing – original draft, writing – review editing, visualization, and funding acquisition. J.A.S. performed methodology, investigation, writing – review editing, and funding acquisition. P.A.L. performed conceptualization, writing – review editing, supervision, and funding Acquisition.

Data Availability Statement

The data that support the findings of this study are available in the supplementary material of this article, and additional data are available upon request or in RADAR4KIT repository: https://doi.org/10.35097/NnKhXXSLSLeHenTi.

Keywords

ferrofluid, Janus carriers, microcargo manipulation, magnetic actuation, programmable microfluidics

Received: April 18, 2024
Revised: June 19, 2024
Published online:

[1] W. Feng, E. Ueda, P. A. Levkin, *Adv. Mater.* **2018**, *30*, 1706111.
[2] L. Nan, H. Zhang, D. A. Weitz, H. Cheung Shum, *Lab Chip* **2024**, *24*, 1135.
[3] R. Malinowski, I. P. Parkin, G. Volpe, *Chem. Soc. Rev.* **2020**, *49*, 7879.
[4] P. Lv, Y.-L. Zhang, D.-D. Han, H.-B. Sun, *Adv. Mater. Interfaces* **2021**, *8*, 2100043.
[5] Q. Sun, D. Wang, Y. Li, J. Zhang, S. Ye, J. Cui, L. Chen, Z. Wang, H.-J. Butt, D. Vollmer, X. Deng, *Nat. Mater.* **2019**, *18*, 936.
[6] W. Wang, H. Vahabi, A. Taassob, S. Pillai, A. K. Kota, *Adv. Sci.* **2024**, *11*, 2308101.
[7] G. Cheng, C. Y. Kuan, K. W. Lou, Y.-P. Ho, *Adv. Mater.* **2024**, 2313935.
[8] Y. Xu, A. M. Rather, Y. Yao, J.-C. Fang, R. S. Mamtani, R. K. A. Bennett, R. G. Atta, S. Adera, U. Tkalec, X. Wang, *Sci. Adv.* **2021**, *7*, eabi7607.
[9] S. Ben, T. Zhou, H. Ma, J. Yao, Y. Ning, D. Tian, K. Liu, L. Jiang, *Adv. Sci.* **2019**, *6*, 1900834.
[10] G. Kwon, D. Panchanathan, S. R. Mahmoudi, M. A. Gondal, G. H. McKinley, K. K. Varanasi, *Nat. Commun.* **2017**, *8*, 14968.
[11] F. W. Du, M. Liu, C. Liu, Q. Zhao, T. Wang, Z. Wang, X. Du, *Sci. Adv.* **2022**, *8*, eabp9369.
[12] A. Li, H. Li, Z. Li, Z. Zhao, K. Li, M. Li, Y. Song, *Sci. Adv.* **2020**, *6*, eaay5808.
[13] J. Zhang, X. Wang, Z. Wang, S. Pan, B. Yi, L. Ai, J. Gao, F. Mugele, X. Yao, *Nat. Commun.* **2021**, *12*, 7136.
[14] S. Jiang, B. Li, J. Zhao, D. Wu, Y. Zhang, Z. Zhao, Y. Zhang, H. Yu, K. Shao, C. Zhang, R. Li, C. Chen, Z. Shen, J. Hu, B. Dong, L. Zhu, J. Li, L. Wang, J. Chu, Y. Hu, *Nat. Commun.* **2023**, *14*, 5455.
[15] Z. Dong, H. Cui, H. Zhang, F. Wang, X. Zhan, F. Mayer, B. Nestler, M. Wegener, P. A. Levkin, *Nat. Commun.* **2021**, *12*, 247.
[16] N. K. Mandsberg, F. Aslan, Z. Dong, P. A. Levkin, *Chem. Commun.* **2024**, *60*, 5872.
[17] T. S. Wong, S. H. Kang, S. K. Y. Tang, E. J. Smythe, B. D. Hatton, A. Grinthal, J. Aizenberg, *Nature* **2011**, *477*, 443.
[18] S. Adera, J. Alvarenga, A. V. Shneidman, C. T. Zhang, A. Davitt, J. Aizenberg, *ACS Nano* **2020**, *14*, 8024.
[19] P.-G. de Gennes, F. Brochard-Wyart, D. Quere, *Capillarity and Wetting Phenomena, Drops, Bubbles, Pearls, Waves*. *1 edn*, Springer-Verlag, New York, **2004**.
[20] J. D. Berry, M. J. Neeson, R. R. Dagastine, D. Y. C. Chan, R. F. Tabor, *J. Colloid Interface Sci.* **2015**, *454*, 226.
[21] M. Latikka, M. Backholm, J. V. I. Timonen, R. H. A. Ras, *Current Opinion in Colloid and Interface Science* **2018**, *36*, 118.
[22] R. E. Rosensweig, Ferrohydrodynamics, Courier Corporation, **2013**.
[23] A. G. Boudouvis, J. L. Puchalla, L. E. Scriven, *Chem. Eng. Commun.* **1988**, *67*, 129.
[24] J. V. I. Timonen, M. Latikka, L. Leibler, R. H. A. Ras, O. Ikkala, *Science* **2013**, *341*, 253.
[25] P. J. Souza, S. H. A. Lira, I. N. de Oliveira, *J. Magn. Magn. Mater.* **2019**, *483*, 129.
[26] U. Banerjee, M. R. Gunjan, S. K. Mitra, *Langmuir* **2024**, *40*, 3105.
[27] X. Fan, X. Dong, A. C. Karacakol, H. Xie, M. Sitti, *Proc. Natl. Acad. Sci. USA* **2020**, *117*, 27916.
[28] A. de Ryck, D. Quéré, *J. Colloid Interface Sci.* **1998**, *203*, 278.
[29] N. K. Mandsberg, A. V. Shneidman, K. H. Jensen, R. Taboryski, L. H. Nielsen, J. Aizenberg, A. Boisen, *Adv. Mater. Interfaces* **2022**, *9*, 2200667.
[30] N. K. Mandsberg, O. Hansen, R. Taboryski, *Sci. Rep.* **2017**, *7*, 12794.
[31] L. Schneider, M. Laustsen, N. Mandsberg, R. Taboryski, *Sci. Rep.* **2016**, *6*, 21400.
[32] N. K. Mandsberg, R. Taboryski, *Surface Topography: Metrology and Propert.* **2017**, *5*, 024001.
[33] L. Duan, X. Ji, Y. Yang, S. Yang, X. Lv, Y. Xie, *RSC Adv.* **2019**, *10*, 1120.
[34] R. A. Deshpande, J. Navne, M. V. Adelmark, E. Shkondin, A. Crovetto, O. Hansen, J. Bachmann, R. Taboryski, *Nat. Commun.* **2024**, *15*, 124.
[35] E. Ueda, P. A. Levkin, *Adv. Mater.* **2013**, *25*, 1234.
[36] A. Einstein, *Naturwissenschaften* **1926**, *14*, 223.
[37] Y. Gu, C. Chen, Z. Mao, H. Bachman, R. Becker, J. Rufo, Z. Wang, P. Zhang, J. Mai, S. Yang, J. Zhang, S. Zhao, Y. Ouyang, D. T. W. Wong, Y. Sadovsky, T. J. Huang, *Sci. Adv.* **2021**, *7*, eabc0467.